Small is beautiful: Upscaling from microscale laminar to natural turbulent rivers

L Malverti, E Lajeunesse, F D Métivier

Small is beautiful: Upscaling from microscale laminar to natural turbulent rivers

L. Malverti,[1] E. Lajeunesse,[1] and F. Métivier[1]

Received 21 December 2007; revised 18 July 2008; accepted 8 August 2008; published 9 October 2008.

[1] The use of microscale experimental rivers (with flow depths of the order of a few millimeters) to investigate natural processes such as alluvial fans dynamics, knickpoints migration, and channel morphologies, such as meandering and braiding has become increasingly popular in recent years. This raises the need to address the issue of how to extrapolate results from the experimental microscale at which flow is laminar to the scale of natural turbulent rivers. We address this question by performing measurements of average flow velocity and sediment transport in an experimental laminar river. The average flow velocity is correctly predicted from the Navier-Stokes equation solved for a steady uniform laminar flow. Laminar sediment transport is found to be consistent with the law of Meyer-Peter and Müller (1948) commonly used to describe sediment transport in natural turbulent rivers. We also show that surface tension is important only if the microscale river width is on the order of or smaller than the capillary length. These results allow us to demonstrate that the evolution of longitudinal bed profiles of turbulent and laminar rivers are governed by identical dimensionless equations and therefore follow the same dynamics. Differences of time and length scales at work in experimental and natural rivers are mainly encoded in the expression of two parameters, a diffusion coefficient and a threshold slope. On the basis of this analysis, we derive a set of equations allowing us to rescale bed elevation, downstream distance, time, and uplift rate from an experimental microscale river to the field scale. Finally, we show how this set of equations can be used to rescale these same parameters in the case of a temporally varying discharge.

Citation: Malverti, L., E. Lajeunesse, and F. Métivier (2008), Small is beautiful: Upscaling from microscale laminar to natural turbulent rivers, *J. Geophys. Res.*, *113*, F04004, doi:10.1029/2007JF000974.

1. Introduction

[2] River and sediment interactions have been the subject of considerable attention in the literature both because of their importance in understanding erosion processes and landscape evolution and because of the many engineering problems associated with river management [*Yalin*, 1977; *Raudkivi*, 1990; *Graf and Altinakar*, 1996]. Rivers are features where a free surface flow occurs in a self formed channel that is both stable and capable of adjusting to variations in flow and sediment transport [*Parker*, 1978a, 1978b].

[3] Solid sediment transport in rivers can be divided into different modes. The first one is the suspended load, consisting of sediment particles small enough to be transported, at least intermittently, by suspension within the flow; it is composed primarily of silt and clay size particles in most rivers [*Allen*, 1985; *Knighton*, 1998]. Sand-size particles can also be part of the suspended load if the stream flow velocity and turbulence are great enough to hold them in suspension. The case where the sediment particles are small enough to remain continuously suspended is usually referred to as wash load. The third transport mode is the bed load consisting of either rolling or saltating particles moving along the bed of a stream. Bed load is primarily composed of the coarser sediment bed particles and plays a key role in the morphodynamics of gravel bed rivers: a large enough portion of the coarse grains composing the bed must indeed be put into motion to achieve a significant evolution of rivers of this type [*Yalin*, 1977; *Graf and Altinakar*, 1996]. In addition, field measurements show that bed load can account for a large fraction of the total mass transported in gravel bed mountain streams [*Wohl*, 2000; *Métivier et al.*, 2004; *Meunier et al.*, 2006].

[4] The evolution of a river bed through bedload transport operates on timescales ranging from 10^{-1} to 10^{4} years, typically too long for us to directly perceive and measure its dynamics [*Knighton*, 1998]. Field measurements and observations of the dynamics of a river bed are also an arduous task [*Peakall et al.*, 1996]. Most of the time, scientists have to be content with estimating bed load transport from measurements of other parameters such as bed morphologies [*Kostaschuk et al.*, 1989] or granulometric distributions that relate to it [*Sklar et al.*, 2006; *Jones and Frostick*, 2008]. This situation has motivated the development of

[1]Laboratoire de Dynamique des Fluides Geologiques, Institut de Physique du Globe de Paris, Paris, France.

0148-0227/08/2007JF000974

Table 1. Comparison Between the Typical Range of Parameters in Froude Scale Models, Microscale Models, and Natural Rivers[a]

Parameters	Froude Scale Models	Microscale Models	Natural Rivers
Flume length (m)	3–160	1–3	–
Flume width (m)	1–4	0.05–2	–
Channel width (m)	0.1–4	10^{-2}–1	1–10^3
Average flow velocity (m/s)	10^{-1}–1	0.05–0.5	0.1–4
H/d	4–10^5	1–40	10–10^5
ρ_s/ρ	≈2.5	≈2.5	≈2.7
Slope	2.10^{-3}–2.10^{-2}	10^{-4}–5.10^{-2}	10^{-6}–10^{-2}
Re	10^3–10^6	100–500	10^4–10^7
Fr	10^{-1}–1	0.5–5	10^{-2}–1
τ^*	10^{-1}–1	0.01–0.8	10^{-2}–10
Experimental duration	0.5–15 days	1–6 h	–

[a]Data on Froude scale models come from *Ashworth et al.* [1994], *Sapozhnikov and Foufoula-Georgiou* [1997], *Lisle et al.* [1997], *Blom et al.* [2003], *Cantelli et al.* [2004], *Carling et al.* [2005], and *Peakall et al.* [2007]. Data on microscale models come from *Métivier and Meunier* [2003] and *Davies et al.* [2003]. Data on natural rivers come from *Bagnold*'s [1980] and *Brownlie*'s [1981] databases. Note that we distinguish the flume width from the channel width. In many cases (e.g., experimental braided rivers), these two parameters may indeed be very different.

experimental channels where sediment-flow interactions and bed morphology can be reproduced and visualized under well-controlled conditions and where the relevant timescales are reduced.

[5] The use of experiments raises the issue of extrapolating from the experimental scale to the field scale. If we neglect suspended load, flow in an alluvial river can be characterized by five dimensionless numbers (see *Peakall et al.* [1996] for a more complete discussion)

$$A = \frac{H}{d}, \tag{1}$$

$$B = \frac{\rho_s}{\rho}, \tag{2}$$

$$Re = \frac{UH}{\nu} = \frac{Q}{\nu}, \tag{3}$$

$$Fr = \frac{U}{\sqrt{gH}}, \tag{4}$$

$$\tau^* = \frac{\tau}{(\rho_s - \rho)gd}, \tag{5}$$

where U is the average flow velocity, H is the flow depth, ν and ρ are the kinematic viscosity and the density of water, Q is the volumetric flow rate per unit river width, τ is the streamwise bed shear stress and g is gravitational acceleration. ρ_s and d are the density and the median diameter of the sediment composing the bed. A is the ratio of flow depth to grain size. B is a density ratio. The Reynolds number Re is the ratio of inertial to viscous forces. Re is very large in natural rivers (typically $Re \gtrsim 10^6$) where flows are almost always turbulent. The Froude number Fr is the ratio of the inertial and gravitational forces, and τ^* is a dimensionless shear stress, called the Shields number [*Shields*, 1936].

[6] Constructing an experimental channel where A, B, Re, Fr, and τ^* would match the values of natural rivers would be the only way to exactly reproduce river dynamics in the lab. In the majority of experiments, the experimental fluid is water. In that case, examination of equations (1)–(5) reveals that scaling can only be achieved on a one to one scale. A compromise must therefore be found that depends on the nature of the problem being investigated. In this regard, two rather different schools of thought have emerged.

[7] The traditional school favors scaling the Froude Number [*Yalin*, 1992; *Peakall et al.*, 1996]. Although smaller than in natural rivers, Re in these experiments is kept sufficiently high to ensure fully turbulent flow. This is achieved by imposing a flow of relatively large dimensions which, in turn, necessitates the use of large experimental flumes typically with widths and lengths of a few meters to a few tens of meters (see Table 1). These experimental rivers exhibit friction coefficients close to natural values and are therefore particularly adapted to the investigation of many engineering problems [*Métivier*, 2003]. This technique known as Froude Scale modeling has for example been successfully applied to modeling rivers with mobile beds and flow interactions with artificial structures such as spillways, conduits and breakwaters [*French*, 1985; *Owen*, 1985]. Because of their relatively large dimensions, Froude scale models often operate on long timescales of a couple of days to several weeks (see Table 1). As a result, they are time consuming when it comes to exploring the sensitivity of the system to a given parameter because this often requires a large number of experimental runs.

[8] The second approach consists of using a class of experiments referred to as "microscale rivers" throughout the rest of the paper. In this approach, Fr, A and B may have values on the order of natural rivers but there is no attempt to achieve high Reynolds numbers. On the contrary, Re is small ($Re \lesssim 200$) and the flow is laminar [*Davies et al.*, 2003]. As result, water flow depth can be reduced down to several mm and small experimental flumes can be used (typically with lengths and widths of a few tens of centimeters to a couple of meters) thus reducing the duration of the experiments (see Table 1).

[9] The microscale approach is subject to several problems. First of all, the flow is not turbulent so that microscale rivers are believed to exhibit unrealistic friction coefficients. Secondly the absence of turbulence prevents suspended load transport so that microscale rivers are irrelevant to investigate field cases where suspension is important. Finally, surface tension may become important at small scales, potentially changing the development and physics of channelized flow.

[10] Although the detailed processes of flow and sediment motion are likely to differ from those at the field scale, many distinct fluvial morphologies can be created by purely laminar flows such as braided rivers (Figure 1) or alluvial fans. *Hong and Davies* [1979], for example, observed that

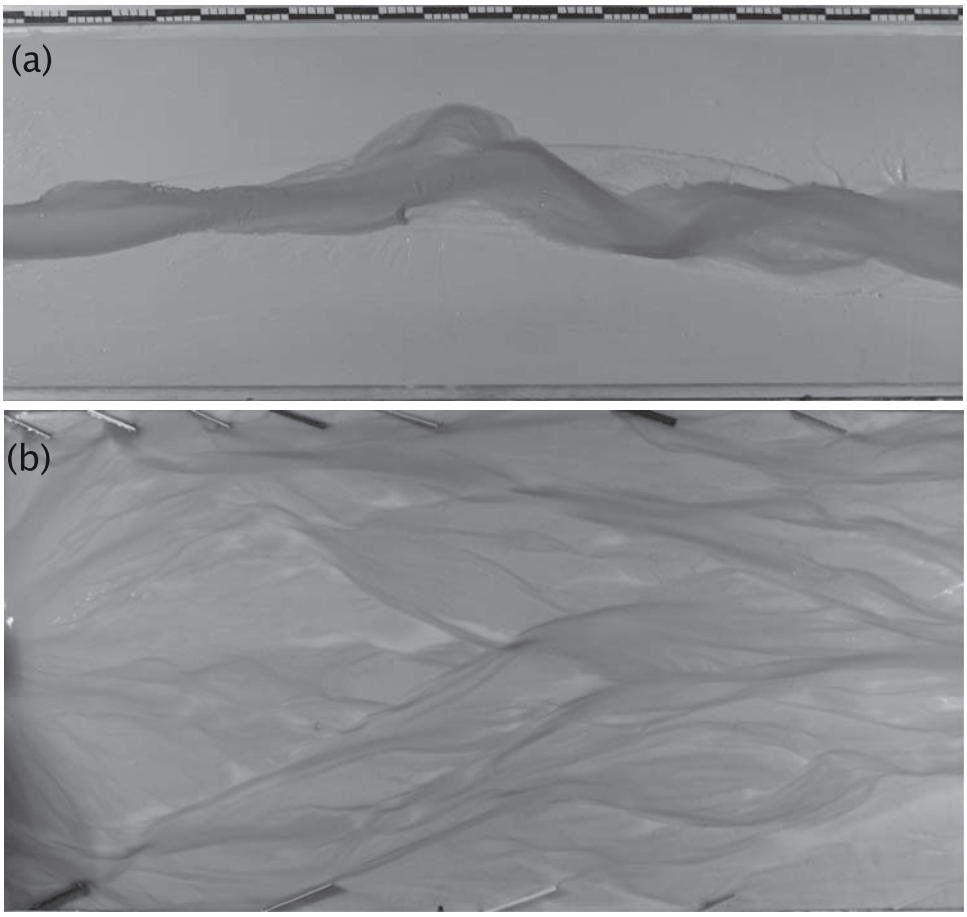

Figure 1. Pictures of two braided microscales laminar rivers in our laboratory by the courtesy of Michal Tal. (a) The average bed slope is 0.015 and the water flow rate is 1 L min^{-1}. The bed is composed of a mixture of 25 and 500 μm glass beads. (b) The average bed slope is 0.025 and the water flow rate is 1.5 L min^{-1}. The bed is composed of 250 μm glass beads. Both photos were taken 4 h after flow initiation. The experimental fluid is water with dye added for visualization. Water flow depth and flow velocities are on the order of a few milimeters and 0.1 m s^{-1}, respectively. Reynolds number varies between 100–500. The flume has a width of 75 cm and a length of 2 m.

the number of braids in a microscale braided river was similar to that in the 1 km wide prototype Rakaia river (New Zealand). Such an experimental approach was also used by *Métivier and Meunier* [2003] to investigate the correlation between input and output sediment fluxes in a microscale braided stream and to show that sediment transport rate can reach steady state even though braiding remains unstable.

[11] Microscale rivers have become increasingly popular to investigate processes such as alluvial fan dynamics [*Hooke*, 1968; *Schumm et al.*, 1987; *Straight*, 1992; *Bryant et al.*, 1995; *Whipple et al.*, 1998; *Parker*, 1999], response of fluviodeltaic systems to base level change [*Koss et al.*, 1994; *Muto and Swenson*, 2005], alluvial-bedrock transitions [*Kim and Muto*, 2007], knickpoints migration [*Malverti et al.*, 2007], braiding [*Meunier and Métivier*, 2000, 2006; *Métivier and Meunier*, 2003] and even anthropogenic aggradation [*Davies et al.*, 2003]. Their appeal lies in the fact that small-scale laminar experiments are indeed easier to set up and they evolve on shorter timescales (typically a few hours) than Froude scale models.

[12] Because turbulence is an ubiquitous feature of flow in rivers, it has long been assumed to strongly influence bed load transport and to determine both the dynamics and morphology of alluvial river beds [*Yalin*, 1992; *Nezu and Nakagawa*, 1993]. It is therefore legitimate to ask questions such as: Can the results obtained from small-scale laminar experiments be extrapolated to the field scale? To what extent can we compare the evolution of the bed of a laminar and a turbulent river? Are the evolutions described by similar equations? And finally, can we extrapolate characteristic time and length scales from the laboratory to the field?

[13] This paper reports a preliminary investigation of this problem and focuses on the evolution of the longitudinal profile of a constant width river bed. We discuss the effect of surface tension and perform experimental measurements of average flow velocity and bed load transport in a microscale laminar river. The results allow us to demonstrate that the evolution of longitudinal bed profiles of turbulent and laminar rivers are governed by identical dimensionless equations and therefore follow the

Table 2. Symbols and Notations Used in This Paper

Symbol	Description	Dimensions
g	gravitational acceleration	$[L][T]^{-2}$
	Natural Turbulent River	
α	numerical constant of the Meyer-Peter and Müller transport law	[0]
Δ	threshold slope (equation of evolution of the natural river bed profile)	[0]
ϕ	volumetric sediment discharge per unit river width	$[L]^2[T]^{-1}$
λ	bed porosity	[0]
ν	kinematic viscosity of water	$[L]^2[T]^{-1}$
ρ	density of water	$[M][L]^{-3}$
ρ_s	density of river bed sediments	$[M][L]^{-3}$
θ	threshold Shield stress of the Meyer-Peter and Müller transport law	[0]
τ	streamwise bed shear stress	$[M][L]^{-1}[T]^{-2}$
τ^*	Shields stress	[0]
c_z	Chézy coefficient	[0]
d	median grain size of the river bed sediments	[L]
D	diffusion coefficient (equation of evolution of the natural river bed profile)	$[L]^2[T]^{-1}$
h	river bed elevation	[L]
H	water flow depth	[L]
Q	volumetric water discharge per unit river width	$[L]^2[T]^{-1}$
R	$(\rho_s - \rho)/\rho$	[0]
Re	Reynolds number of natural river, $UH/\nu = Q/\nu$	[0]
S	river bed slope, $-\partial h/\partial x$	[0]
t	time	[T]
U	average flow velocity	$[L][T]^{-1}$
U_p	uplift rate	$[L][T]^{-1}$
x	downstream distance	[L]
	Laminar Microscale River	
α_L	numerical constant of the Meyer-Peter and Müller transport law	[0]
Δ_L	threshold slope (equation of evolution of the laminar river bed profile)	[0]
ϕ_L	volumetric sediment discharge per unit river width	$[L]^2[T]^{-1}$
λ_L	bed porosity	[0]
ν_L	kinematic viscosity of the experimental fluid	$[L]^2[T]^{-1}$
ρ_L	density of the experimental fluid	$[M][L]^{-3}$
ρ_{sL}	density of the microscale river bed sediments	$[M][L]^{-3}$
θ_L	threshold Shield stress of the Meyer-Peter and Müller transport law	[0]
σ	surface tension between air and the experimental fluid	$[M][T]^{-2}$
τ_L	streamwise bed shear stress	$[M][L]^{-1}[T]^{-2}$
τ^*_L	Shields stress	[0]
B_{oc}	channel Bond number, $\rho_L g W_L^2/\sigma$	[0]
d_L	median grain size of the microscale river bed sediments	[L]
D_L	diffusion coefficient (equation of evolution of the laminar river bed profile)	$[L]^2[T]^{-1}$
h_L	microscale river bed elevation	[L]
H_L	water flow depth	[L]
Q_L	volumetric water discharge per unit river width	$[L]^2[T]^{-1}$
r_c	curvature radius of the fluid/air interface	[L]
R_L	$(\rho_{s,L} - \rho_L)/\rho_L$	[0]
Re_L	Reynolds number of the microscale river, $U_L H_L/\nu_L = Q_L/\nu_L$	[0]
S_L	microscale river bed slope, $-\partial h_L/\partial x_L$	[0]
t_L	time	[T]
U_L	average flow velocity	$[L][T]^{-1}$
U_{pL}	artificial uplift rate	$[L][T]^{-1}$
W_L	microscale river width	[L]
x_L	downstream distance	[L]
y_L	distance along transverse flow direction	[L]

same dynamics. On the basis of this analysis, we derive a set of equations allowing us to rescale bed elevation, downstream distance, time and uplift rate from an experimental microscale river to the field scale. We also show how this set of equations can be used to rescale these same parameters in the case of a temporally varying discharge.

2. Longitudinal Profile of a Turbulent Alluvial River

[14] In this section, we follow the same arguments as previous investigations [*Begin et al.*, 1981; *Paola et al.*, 1992; *Parker et al.*, 1998; *Métivier*, 1999] to derive the equation governing the evolution of the longitudinal profile of a turbulent alluvial river. In order to keep a simple analytical formalism, we restrict ourselves to the simplified case of a 2-D alluvial river of constant width and we neglect lateral inflow of both sediment and water. The following discussion can easily be modified to account for such effects. Symbols and notations used in the paper are summarized in Table 2.

[15] Conservation of water reduces to

$$Q = UH. \tag{6}$$

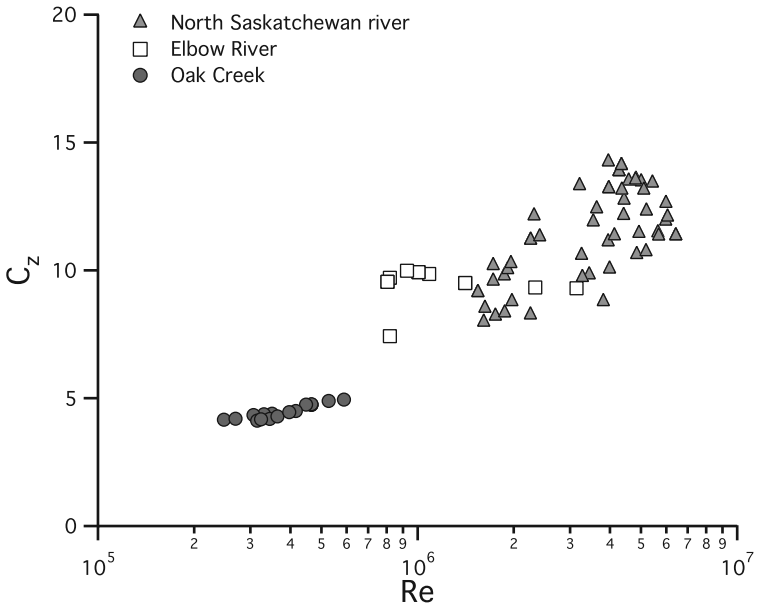

Figure 2. Chézy coefficient c_z as a function of *Re* for several gravel bed rivers: the North Saskatchewan River (triangles), the Elbow River (squares), and the Oak Creek River (circles). Data correspond to rivers with beds of median diameter larger than 2 mm. They are extracted from *Bagnold*'s [1980] and *Brownlie*'s [1981] databases. For each river, only one given site is considered.

For sufficiently long space and timescales, the flow is assumed to be stationary and uniform and momentum conservation can be written as

$$\tau = \rho g H S, \tag{7}$$

where $S = -\partial h/\partial x$ is the bed slope, h is the elevation of the sediment bed surface relative to a fixed horizontal datum, and x is the downstream distance (positive downstream with $x = 0$ at the inlet).

[16] For an open channel turbulent flow, it is common practice to relate H and U by a friction relation such as the Chézy formula [*Yalin*, 1992]

$$U = c_z \sqrt{gHS}, \tag{8}$$

where c_z is a dimensionless coefficient called the Chézy coefficient. Although c_z is a function of H, this dependance is weak [*Keulegan*, 1938; *Parker*, 1991]. For example, *Parker* [1991] predicts $c_z \propto H^{1/6}$ so that a fourfold increase in water flow depth only increases the Chézy coefficient by a factor of 1.26. This weak dependency has been confirmed by field measurements, at least in the case of gravel bed rivers [*Meunier et al.*, 2006]. The Chézy coefficient measured on several gravel bed rivers is plotted as a function of *Re* in Figure 2: variations of c_z at a given site on a given river are small. In the following analysis, c_z will therefore be assumed constant.

[17] Sediment mass conservation is formulated by the Exner equation

$$(1-\lambda)\frac{\partial h}{\partial t} + \frac{\partial \Phi}{\partial x} = U_p, \tag{9}$$

where t denotes time, λ is the bed porosity, Φ is the volumetric sediment discharge per unit river width and U_p is the tectonic uplift rate (subsidence would be modeled by a negative U_p).

[18] There is no explicit equation available for momentum conservation of sediments being transported as bed load. A large number of equations have been proposed to describe bed load sediment transport in alluvial rivers [*Gessler*, 1971; *Carson and Griffiths*, 1987; *Gomez and Church*, 1989; *Dietrich et al.*, 2003], many of them with a low rate of success [*Wohl*, 2000]. Establishing a universal bed load transport equation or discussing the validity of the ones available in the literature remain active subjects of research but are beyond the scope of this paper. Therefore we chose to use a well founded semiempirical relation for this analysis. The most commonly used is the transport law of *Meyer-Peter and Müller* [1948] which takes the form [*Paola et al.*, 1992]

$$\frac{\Phi}{(R \cdot g \cdot d^3)^{1/2}} = \begin{cases} \alpha(\tau^* - \theta)^{3/2} & for \quad \tau^* \geq \theta \\ 0 & for \quad \tau^* < \theta, \end{cases} \tag{10}$$

where $R = (\rho_s - \rho)/\rho$, α is a dimensionless coefficient and θ is a dimensionless threshold shear stress below which no sediment is transported. Meyer-Peter and Müller derived equation (10) from flume data pertaining to well-sorted sediment in the gravel size range. A fit of the data by equation (10) resulted in $\alpha = 8$ and $\theta = 0.047$ [*Meyer-Peter and Müller*, 1948]. The data were later reanalyzed by *Wong* [2003] who found $\alpha = 3.97$ and $\theta = 0.0495$.

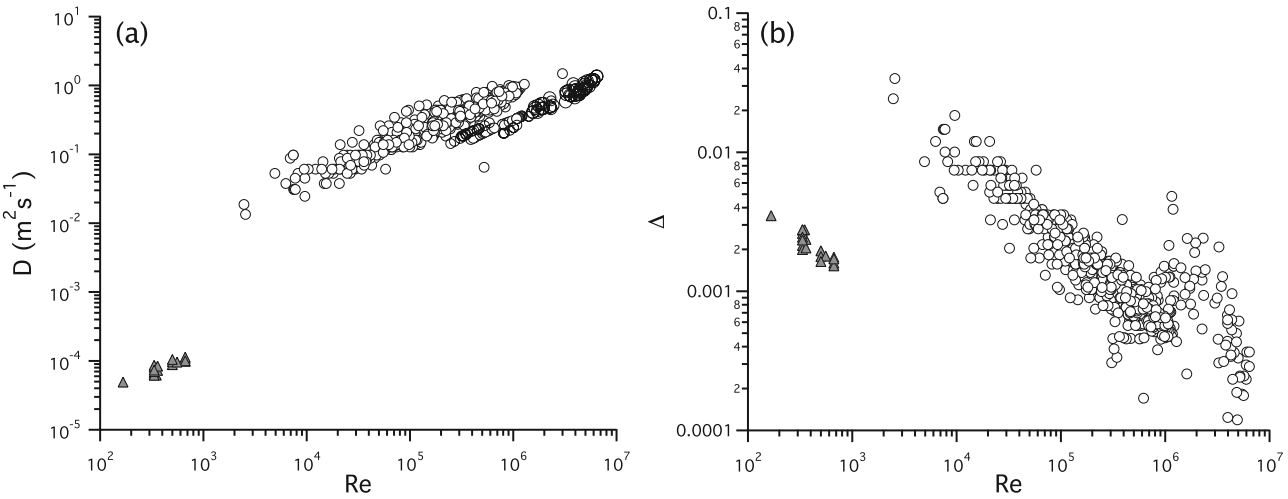

Figure 3. (a) Diffusion coefficient and (b) threshold slope as a function of the Reynolds number *Re* for several natural turbulent rivers (circles) and laminar microscale rivers (triangles). Natural data come from *Bagnold*'s [1980] and *Brownlie*'s [1981] databases and from measurement acquired by our group [*Métivier et al.*, 2004; *Liu et al.*, 2008] in the Urümqi river (Chinese Tian-Shan). They all pertain to rivers with beds of median diameter larger than 2 mm.

[19] Combining equations (6)–(10) leads to the equation governing the evolution of the 2-D profile of the bed of a turbulent river

$$(1-\lambda)\frac{\partial h}{\partial t} = \begin{cases} U_p - D\frac{\partial}{\partial x}\left[\left(-\frac{\partial h}{\partial x}\right)^{2/3} - \Delta^{2/3}\right]^{3/2} \\ \qquad \text{for } -\frac{\partial h}{\partial x} \geq \Delta \\ U_p \qquad \text{for } -\frac{\partial h}{\partial x} \leq \Delta, \end{cases} \tag{11}$$

where D is a diffusion coefficient and Δ is a threshold slope below which no sediment is transported

$$D = \alpha \frac{Q}{Rc_z} \tag{12}$$

$$\Delta = c_z \frac{\left(R^3 d^3 \theta^3 g\right)^{1/2}}{Q}. \tag{13}$$

[20] The evolution of the bed of an alluvial turbulent river is therefore described by the nonlinear diffusion equation (11) with two parameters D and Δ. Figure 3 shows typical values of these parameters. Δ varies between 10^{-4} and 10^{-2} and D between 10^{-2} and 10 m^2s^{-1}.

[21] Note that equation (11) is valid for a flat bed. In the presence of bedforms such as dunes or bars, both the friction equation (8) and the expression of the Shields stress need to be modified to account for the effect of form drag (see for example [*Wright and Parker*, 2004]). This might affect the values of the exponents in equation (11). Such an effect is however beyond the scope of the present paper. Finally we note that when the slope of a river is large compared to Δ, the latter can be neglected thus reducing equation (11) to a linear diffusion equation (see *Paola* [2000] for a detailed discussion of the conditions under which this approximation is valid)

$$\frac{\partial h}{\partial t} = U_p + D\frac{\partial^2 h}{\partial x^2}. \tag{14}$$

3. Evolution of the Longitudinal Profile of a Microscale Laminar Alluvial River

[22] We now turn toward the case of experimental microscale rivers and examine what equations govern the evolution of their longitudinal profile. To distinguish between the characteristics of laminar and turbulent rivers, all parameters associated with experimental laminar rivers will be denoted by an index (L).

[23] Because the flow in a microscale river is laminar, both the sediment transport law and the friction equation are likely to be different from the natural turbulent case discussed in the previous section. This was investigated through several series of experiments dedicated to the measurement of the sediment transport law and the relation between slope, flow depth and velocity which are described in the following sections. The effect of surface tension is also addressed.

3.1. Experimental Setup and Procedure

[24] Our experiments were carried out in a small inclinable flume of width $W_L = 0.05$ m and length 0.9 m schemed in Figure 4. The experimental procedure consisted of preparing a flat sediment bed several centimeters thick (typically 8 cm) for which the slope S_L was measured with a digital inclinometer (accuracy 0.1°). The experimental sediment consisted of small glass beads of density ρ_{sL} = 2500 kg m^{-3}. Measurements of the sediment grain size distribution using a magnifying lens showed that it has a gaussian form peaked around the median grain size d_L = 75μm with D_{10} = 50μm and D_{90} = 90μm.

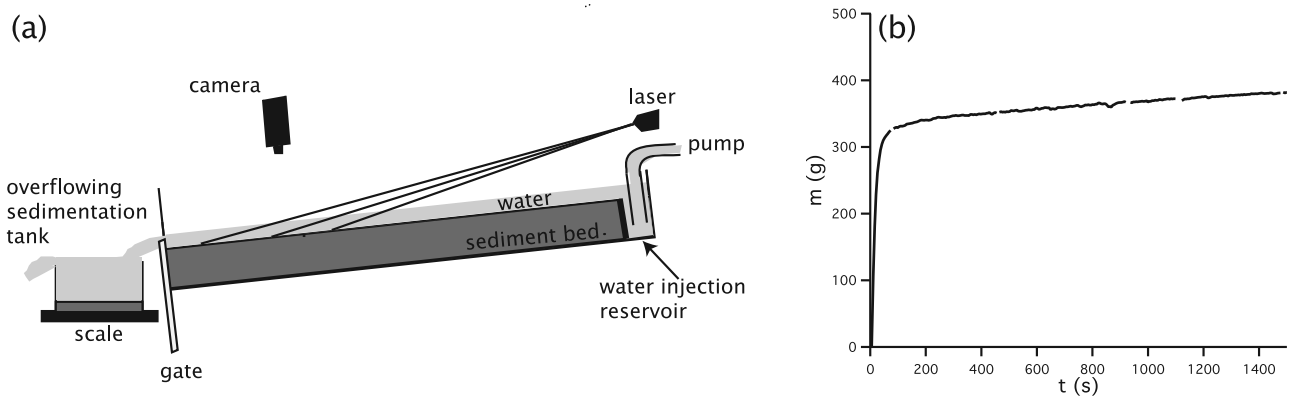

Figure 4. (a) Schematic of the experimental setup. (b) Cumulative sediment mass as a function of time at the flume outlet for $Q_L = 5.10^{-4}$ m^{2}s^{-1} and $S = 0.035$ (2°). The same qualitative behavior was observed in all experiments. The initiation of the flow was followed by a transitory during which the mass of sediment collected at the flume outlet increased rapidly. After about 2 min, a stationary state was reached characterized by a linear increase of the cumulative sediment mass with time which indicates a constant sediment discharge.

[25] Once the bed was ready, the fluid was injected by a pump at the upstream flume inlet with a constant discharge per unit river width Q_L measured with a flow meter (accuracy 0.01 L min^{-1}). To prevent any disturbance of the bed, the fluid was not injected as a point source but rather it overflowed smoothly onto the river bed via a small reservoir (see Figure 4). The reservoir extended across the full 5 cm width of the channel and therefore guaranteed a flow injection that was uniform across the channel width. In all the experimental runs the discharge was high enough for the flow to form across the full width of the flume. The fluid used in the experiments was water, but for the sake of generality, we will denote ν_L and ρ_L as the kinematic viscosity and the density of the experimental fluid. The following discussion is therefore pertinent for any experiments which involve any fluid other than water.

[26] Sediment particles transported by the flow settled out in a constant water level overflow tank located at the flume outlet. The tank rested on a high-precision scale (accuracy 0.1 g) connected to a computer that recorded the weight every 10 s. The sediment discharge per unit river width Φ_L was then deduced from the sediment cumulative mass (Figure 4b).

[27] The initiation of the flow was followed by a transitory phase during which the mass of sediment collected at the flume outlet increased rapidly. After about two minutes, a steady state was reached characterized by a linear increase in the cumulative sediment mass with time indicating a constant sediment discharge (Figure 4b). All the experimental measurements described hereafter were performed during this steady state regime. Because we did not feed sediment at the river inlet, an erosion wave slowly propagated from the inlet toward the outlet of the flume. All our experiments were stopped well before this degradation wave had reached the middle of the flume where we performed our measurements so that it never interfered with our results. Indeed the slope of the river bed measured at the end of the experiment was equal to the initial slope within the experimental accuracy.

[28] We performed a large number of experimental runs in which we varied the water flow rate between 0.1 and 2 L/minute and S_L between 0.3 and 3°. As a result, Reynolds number $Re_L = Q_L/\nu_L$ varied between 100 and 300 and remained below 500 which is the value of transition to turbulent flows for an open channel flow. The flow in our experimental river was therefore laminar.

[29] It should be noted that for the range of Re_L explored in our experiment, the nature of the flow is also sensitive to bed roughness. If the latter becomes important relative to flow depth, it may trigger the transition from a laminar to a turbulent flow. As an example, we performed several experimental runs using 350 μm diameter glass beads and observed that the flow was weakly turbulent.

[30] The surface flow velocity U_s was measured by tracking the motion of small floating tracer plastic particles entrained by the flow. Digital images of the particles were acquired at a rate of 25 images per second using a digital camera (576 × 720 pixels) placed vertically above the flume and achieving a spatial resolution of 0.5 mm per pixel. The images were used to compute the surface flow velocity U_s with a relative accuracy of 1%. Given that the flow is laminar, it is expected to obey a Poiseuille velocity profile. The averaged velocity U_L was therefore calculated as in a Poiseuille flow $U_L = 2\ U_s/3$, an assumption that was justified by our experimental results as discussed below.

[31] From conservation of water

$$Q_L = U_L H_L, \tag{15}$$

we deduced the average flow depth $H_L = Q_L/U_L$. The accuracy of the determination of H_L mainly depended on the accuracy of the water flow rate measurement and varied between 0.5% at large flow rates and 10% at low flow rate.

[32] H_L was found to vary between 1 and 3 mm in our experiments. Such values were too small to allow us to measure flow depth directly using methods like the deviation of a laser sheet. Therefore we were not able to check for flow uniformity by checking for constant flow depth. However close examination of the bed showed that it remained flat for the whole duration of the experiment in the range of parameters explored. Direct observation of the

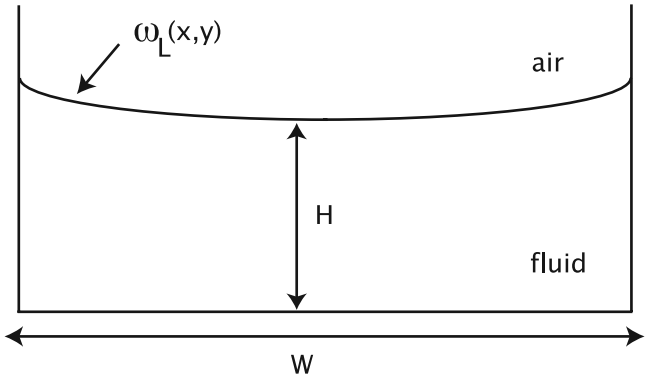

Figure 5. Cross-sectional scheme of the interface ω_L between fluid and air.

flow surface showed that it remained smooth and flat except in the immediate vicinity of the sidewalls where a small meniscus of size about 1 mm developed because of wetting of the glass sidewalls by the experimental fluid [*Degennes*, 1985]. This observation raises the important issue of the effect of surface tension on small-scale experimental flumes which is addressed in the next section.

3.2. Influence of Surface Tension

[33] Surface tension σ is a tensile force which results from the difference between the internal molecular forces of a liquid and the forces between liquid molecules and an adjacent surface. Surface tension varies as a function of temperature [*Lajeunesse and Homsy*, 2003]. It acts only at the free surface; consequently, it does not appear in the Navier-Stokes equations, but rather enters through the boundary conditions [*Guyon et al.*, 2001].

[34] In rivers, the effect of surface tension is largely insignificant [*Peakall et al.*, 1996]. In microscale rivers, however, flow depth is small and surface tension may become important. *Peakall and Warburton* [1996] and *Métivier and Meunier* [2003] concluded on the basis of dimensional analysis that the effect of surface tension is negligible as long as the dimensionless Weber number $W_b = \rho_L U_L^2 H_L/\sigma$ is large. In our experiments, W_b typically ranged between 0.1 and 2, suggesting that surface tension may have influenced the dynamics of our microscale river. This was however not the case as we shall now demonstrate by including explicitly the surface tension term into Saint-Venant equations for a microscale river.

[35] Surface tension acts by creating a pressure jump ΔP at the interface ω_L between fluid and air (see Figure 5)

$$\Delta P = \frac{\sigma}{r_c}, \tag{16}$$

where σ is the surface tension between the air and the experimental fluid and r_c is the radius of curvature of the fluid-air interface. If the slope of the fluid-air interface is small, r_c is given by

$$r_c \approx \left(\frac{\partial^2 \omega_L}{\partial x_L^2} + \frac{\partial^2 \omega_L}{\partial y_L^2}\right)^{-1}, \tag{17}$$

where x_L is the downstream distance and y_L the distance along the transverse flow direction. This pressure jump modifies the pressure field P_L in the river which now depends on the local curvature of the fluid-air interface

$$P_L(z_L) = \rho g(H_L - z_L) - \frac{\sigma}{r_c}, \tag{18}$$

where z_L is the vertical coordinate. Note that the magnitude of the effect of surface tension is controlled by the curvature of the water free surface. If this surface is flat, the curvature cancels and the pressure jump due to surface tension vanishes. We need therefore to consider the general situation of a curved (nonzero curvature) fluid-air interface to correctly evaluate the effect of surface tension. This is why we now write Saint-Venant equation for the most general case of an unsteady and nonuniform laminar river and include the effect of surface tension

$$\rho_L \frac{\partial (U_L H_L)}{\partial t_L} + \rho_L \frac{\partial \left(U_L^2 H_L\right)}{\partial x_L} = \rho_L g H_L S_L - \tau_L - \frac{\partial}{\partial x_L}\left[\rho_L g H_L^2 \left(1 - \frac{\sigma}{\rho_L g H_L r_c}\right)\right], \tag{19}$$

where τ_L is the basal shear stress exerted by the river on the sediment bed.

[36] The effect of surface tension is encoded in the ratio $\sigma/\rho_L\ H_L\ r_c$ which expresses the local ratio between the hydrostatic pressure and the pressure jump due to surface tension. From equation (17), we see that

$$r_c \propto \left(\frac{H_L}{\xi^2} + \frac{H_L}{W_L^2}\right)^{-1}, \tag{20}$$

where W_L is the width of the laminar river and ξ is a characteristic length along the streamwise direction. The fluid surface of our laminar river did not exhibit any structures such as a hydraulic jump and therefore ξ is typically on the order of the flume length. As a result $\xi \gg W_L$ which leads to

$$r_c \propto \frac{W_L^2}{H_L} \tag{21}$$

and therefore

$$\frac{\sigma}{\rho_L H_L r_c} \propto \frac{\sigma}{\rho_L g W_L^2}. \tag{22}$$

The magnitude of surface tension effects is therefore described by a dimensionless parameter, which we will call the channel Bond number because of its resemblance to the Bond number commonly used in interfacial fluid mechanics [*Guyon et al.*, 2001]

$$B_{oc} = \frac{\rho_L g W_L^2}{\sigma} = \frac{W_L^2}{l_c^2}, \tag{23}$$

where $l_c = \sqrt{\sigma/\rho_L g}$ is the capillary length of the experimental fluid. Surface tension becomes important for $B_{oc} \lesssim 1$.

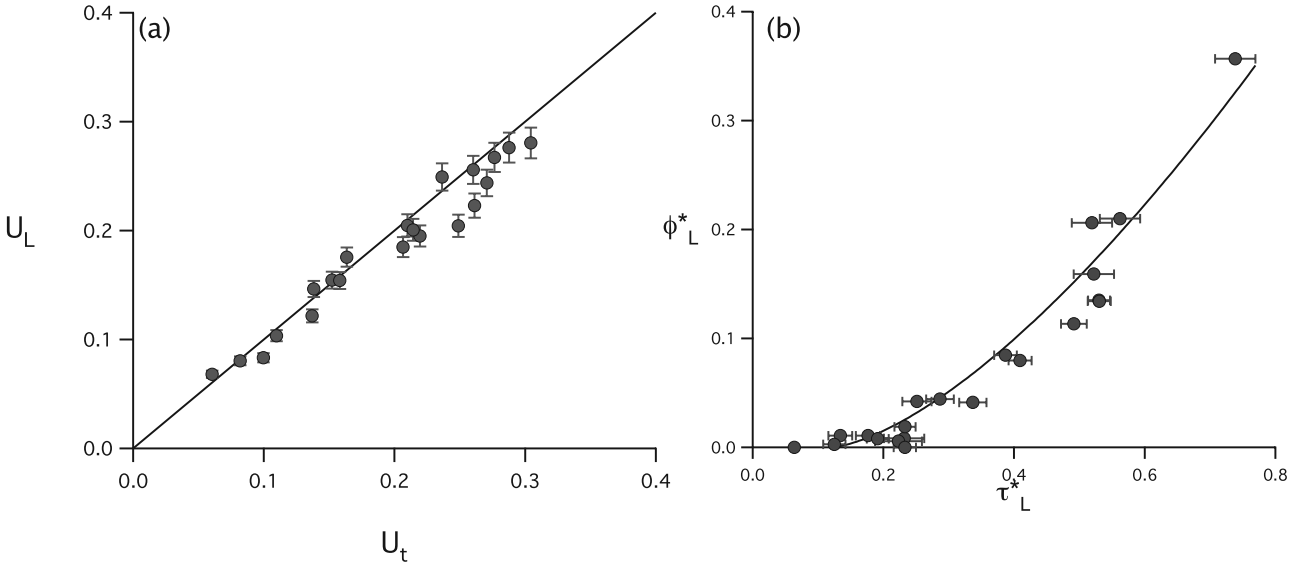

Figure 6. (a) Average flow velocity U_L as a function of the predicted values using equation (24) $U_t = (gS_L{Q_L}^2/3\nu_L)^{1/3}$. The solid line corresponds to a linear fit of the experimental data. (b) Dimensionless sediment transport rate $\Phi_L{}^* = \Phi_L/(R_L g {d_L}^3)^{1/2}$ as a function of the Shields number $\tau_L{}^*$. The solid line corresponds to a fit of the experimental data to the Meyer-Peter and Müller law.

[37] To summarize, surface tension acts only for a curved (nonzero curvature) fluid-air interface. Even though its effect becomes important at small B_{oc}, i.e., when the microscale river width becomes on the order of or smaller than the capillary length. For water within air, this latter is 2.6 mm. In our experiment, $B_{oc} \approx 370$ and surface tension was therefore negligible.

[38] Let us end with three important remarks. First of all, the previous analysis made no assumption about the flow and holds for both laminar and turbulent flows. It suggests that the dimensionless parameter B_{oc} is more appropriate than the Weber number to estimate the influence of surface tension on the flow in a laminar microscale river. Secondly, a microscale river of width on the order of l_c is likely to be strongly influenced by surface tension. The above discussion therefore indicates that small-scale experiments are probably not suitable to investigate the early stages of channel inception for which the width of the channel is small. Finally, let us point out that the previous analysis mainly focuses on the influence of surface tension on the basal shear stress exerted by a microscale river on its bed. We have not discussed how surface tension influences erosion and boundary conditions along the banks. A full analysis of the impact of surface tension on the morphology of an erodible bank microscale river remains to be done although the experimental results of *Métivier and Meunier* [2003] suggest that this effect is weak.

3.3. Friction Equation in a Laminar Microscale River

[39] Let us now turn to the friction equation in our laminar river. As argued in section 3.1, we used our laminar experimental river in a range of parameters for which the flow was uniform. The discussion held in section 3.2 also shows that surface tension was negligible. Sidewall friction which scales as $(H_L/W_L)^2 \approx 10^{-2}$ is therefore assumed negligible. Solving the Navier-Stokes equation for a steady uniform laminar flow in an open channel neglecting both surface tension and sidewall friction leads to the following relationship:

$$U_L = \left(\frac{gS_L Q_L^2}{3\nu_L}\right)^{1/3}. \tag{24}$$

[40] A linear fit of our experimental data leads to $U_L = 0.95\,(gS_L Q_L^2/3\,\nu_L)^{1/3}$ (see Figure 6a). Taking into account the experimental uncertainties, our data exhibit a rather good agreement with the values predicted from (24).

[41] This agreement between the calculated and the measured velocities has important consequences: (1) it validates the assumption of a steady uniform flow, (2) it confirms the laminar nature of the flow in our microscale river, and (3) it demonstrates that surface tension and sidewall friction have a minor impact on the flow.

3.4. Sediment Transport Law in a Laminar Microscale River

[42] Let us now discuss the sediment transport law in a laminar microscale river. Equation (19) leads to the following expression for the streamwise bed shear stress in a steady uniform flow

$$\tau_L = \rho_L g H_L S_L. \tag{25}$$

The corresponding Shields number is

$$\tau_L^* = H_L S_L / R_L d_L, \tag{26}$$

where $R_L = (\rho_{sL} - \rho_L)/\rho_L$.

[43] Measurements of Φ_L as a function $\tau_L{}^*$ are reported in Figure 6b. A fit of our experimental data shows that sediment transport in a laminar river is compatible with a

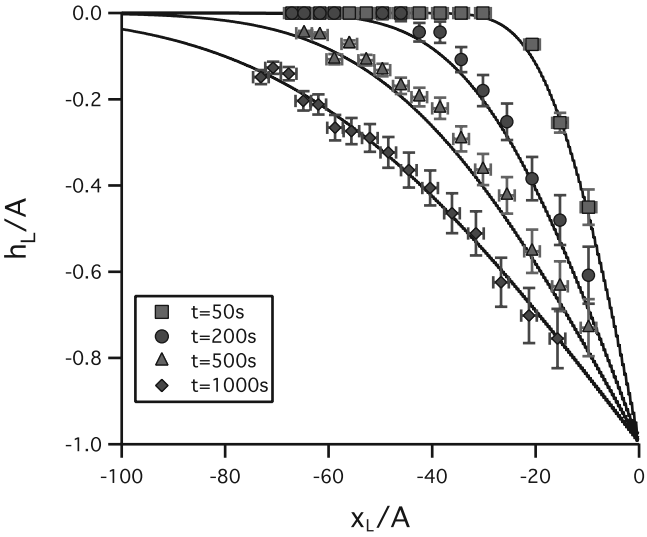

Figure 7. Bed elevation as a function of downstream distance for an experimental run with an initial bed slope of 0.035, an offset of amplitude A = 0.5 mm, and a critical slope Δ_L = 0.003. Bed elevation h_L and downstream distance x_L are normalized to the offset amplitude A. Symbols correspond to experimental data acquired at different times as indicated in the inset. Solid lines correspond to the predictions of equation (29).

transport model such as that of Meyer-Peter and Müller, as in the case of natural rivers

$$\frac{\Phi_L}{\left(R_L \cdot g \cdot d_L^3\right)^{1/2}} = \begin{cases} \alpha_L\left(\tau_L^* - \theta_L\right)^{3/2} & for \quad \tau_L^* \geq \theta_L \\ 0 & for \quad \tau_L^* < \theta_L, \end{cases} \tag{27}$$

with α_L = 0.67 and θ_L = 0.12.

[44] Although θ_L is calculated as a fitting parameter, it exhibits good agreement with the Shields number measured at the onset of sediment motion determined from direct visualization. It is also in good agreement with the critical Shields number 0.07 predicted from the Shields curve for the experimental range of grain Reynolds numbers $Re^* = \sqrt{gd_L}d_L/\nu_L$ = 2.5 [*Shields*, 1936].

[45] We do not imply that the Meyer-Peter and Müller equation is the only one capable of predicting our experimental data. The situation is rather similar to the one previously discussed for natural rivers: the experimental data could certainly be described by slightly different transport laws with slightly different exponents, numerical constants and thresholds such as the one proposed by [*Charru et al.*, 2004]. A discussion of which law best fits the data is an objective of our future work. For the purpose of the present paper, it is sufficient to note that sediment transport in a laminar river is compatible with a law of the Meyer-Peter and Müller type.

3.5. Governing Equation for the Longitudinal Profile of an Alluvial Laminar River

[46] For a microscale river with no lateral inflow of sediment and a constant width, sediment mass conservation goes as

$$(1-\lambda_L)\frac{\partial h_L}{\partial t_L} + \frac{\partial \Phi_L}{\partial x_L} = U_{pL}, \tag{28}$$

where λ_L and h_L are the bed porosity and elevation respectively of the microscale river. t_L denotes time for a microscale experiment. Several authors have attempted to model the effect of tectonic uplift, subsidence or sea level variations in a microscale river by modifying the base level during an experimental run [see, e.g., *Paola et al.*, 2001; *Muto and Swenson*, 2005]. In order to deal with the most general case, we therefore introduce an artificial "uplift rate" U_{pL} in equation (28).

[47] Equations (15), (24), (25), (27), and (28) lead to the equation governing the evolution of the profile of a 2-D laminar river

$$(1-\lambda_L)\frac{\partial h_L}{\partial t_L} = \begin{cases} U_{pL} - D_L \frac{\partial}{\partial x_L}\left[\left(-\frac{\partial h_L}{\partial x_L}\right)^{2/3} - \Delta_L^{2/3}\right]^{3/2} \\ \qquad for -\frac{\partial h_L}{\partial x_L} \geq \Delta_L \\ U_{pL} \qquad for -\frac{\partial h_L}{\partial x_L} \leq \Delta_L \end{cases}. \tag{29}$$

D_L is a diffusion coefficient and Δ_L is a threshold slope defined by

$$D_L = \frac{\alpha_L}{R_L} \cdot \sqrt{3\nu_L Q_L} \tag{30}$$

$$\Delta_L = \left(\frac{R_L^3 d_L^3 g \theta_L^3}{3\nu_L Q_L}\right)^{1/2}. \tag{31}$$

3.6. Experimental Verification

[48] We performed a series of experimental run in order to verify that a constant width laminar river indeed obeys the nonlinear diffusion equation (29). These experiments were performed using the setup previously described in section 3.1. The procedure consisted to perturb an initially uniform river bed by creating a vertical offset. This offset was imposed using a gate located at the downstream end of the flume which can be dropped down so rapidly in comparison to the timescale of channel evolution that it can be considered as instantaneous (Figure 4). The response of the river to this sudden perturbation was measured by mean of a set of laser sheets projected onto the river bed. A digital camera positioned above and perpendicular to the bed recorded images of the laser sheets the deviation of which allowed us to measure the variations of bed elevation within an accuracy of 6%. The size of the region imaged by the camera was about 40 cm. Note that there was no sediment input at the river inlet. As a result an erosion wave progressively propagated slowly from the inlet toward the outlet of the flume. All our experiments were stopped before this degradation wave had reached the region of interest so that it never interfered with our results (see *Malverti et al.* [2007] for more details on the experimental procedure).

[49] Several series of experimental runs were conducted with initial bed slope ranging from 0.3° to 4°, water discharge from 0.5 to 2.5 L min^1 and offset from 0.5 to 1 cm. Experimental duration ranged between 30 min and 1 h. Figure 7 displays the evolution of the bed elevation

observed for a typical experimental run. The river responded to the offset by spreading a diffusive erosion wave upstream.

[50] Equation (29) was solved numerically using a finite difference scheme for all experimental runs. It showed a very good agreement with the experimental data (as illustrated on Figure 7) thus confirming the validity of equation (29) to describe the longitudinal profile of a laminar constant width river.

[51] To be complete, it is important to note that the agreement between the predictions of equation (29) and the experiments was good provided that the amplitude of the offset was smaller or on the order of the water depth H_L. When the offset amplitude was much larger than H_L, the uniform flow assumption was not met any more so that equation (29) failed to capture the first instants of the erosion of the scarp.

4. Discussion

[52] Equation (29) which describes the dynamics of a microscale river longitudinal profile is similar to equation (11) derived for a natural river. The differences between a turbulent and a laminar river are encoded in the expressions of the diffusion coefficients and the threshold slopes. We now discuss in details how these coefficients can be used to upscale from microscale laminar to natural turbulent rivers.

[53] Let us start with natural rivers. Equation (11) which describes the evolution of longitudinal profile of a constant width natural river can be made dimensionless by defining the following dimensionless variables:

$$h^* = \frac{h}{\ell\Delta}, \tag{32}$$

$$x^* = \frac{x}{\ell}, \tag{33}$$

$$t^* = \frac{D}{(1-\lambda)\ell^2}\,t, \tag{34}$$

where ℓ is some characteristic river length. The choice of ℓ depends on the problem under investigation: ℓ could be the river length if one studies the long-term evolution of a complete river profile; it could be the length of a reach if one is to investigate the river profile at a more local scale. With these new variables, equation (11) becomes

$$\frac{\partial h^*}{\partial t^*} = \begin{cases} U_p^* - \dfrac{\partial}{\partial x^*}\left[\left(-\dfrac{\partial h^*}{\partial x^*}\right)^{2/3} - 1\right]^{3/2} \\ \qquad for\ -\dfrac{\partial h^*}{\partial x^*} \geq 1 \\ U_p^* \qquad for\ -\dfrac{\partial h^*}{\partial x^*} \leq 1, \end{cases} \tag{35}$$

where U_p* is a dimensionless uplift rate defined as

$$Up^* = \frac{Up\ \ell}{D\Delta}. \tag{36}$$

In equation (35), the downstream distance is measured in units of ℓ, slope is measured in units of the critical slope Δ and time is measured in units of the characteristic diffusive time $\tau_D = (1 - \lambda)\ell^2/D$.

[54] The same procedure can be applied to equation (29) which describes the evolution of a laminar river bed profile, leading to the dimensionless equation

$$\frac{\partial h_L^*}{\partial t_L^*} = \begin{cases} U_{pL}^* - \dfrac{\partial}{\partial x_L^*}\left[\left(-\dfrac{\partial h_L^*}{\partial x_L^*}\right)^{2/3} - 1\right]^{3/2} \\ \qquad for\ -\dfrac{\partial h_L^*}{\partial x_L^*} \geq 1 \\ U_{pL}^* \qquad for\ -\dfrac{\partial h_L^*}{\partial x_L^*} \leq 1, \end{cases} \tag{37}$$

involving the following dimensionless variables and parameters

$$h_L^* = \frac{h_L}{\ell_L\Delta_L}, \tag{38}$$

$$x_L^* = \frac{x_L}{\ell_L}, \tag{39}$$

$$t_L^* = \frac{D_L}{(1-\lambda_L)\ell_L^2}\,t_L, \tag{40}$$

$$U_{pL}^* = \frac{U_{pL}\ \ell_L}{D_L\Delta_L}, \tag{41}$$

where ℓ_L is some characteristic length of the laminar river.

[55] Under their dimensionless shape, equations (35) and (37) are strictly identical. If solved for the same dimensionless boundary and initial conditions, they will lead to the same dimensionless solution

$$h^*(x^*, t^*) = h_L^*\left(x_L^*, t_L^*\right)\ provided \begin{cases} x^* = x_L^* \\ t^* = t_L^* \\ U_p^* = U_{pL}^*. \end{cases} \tag{42}$$

From the above equation, it follows that upscaling from the time and length scales of a microscale experiment to that of natural rivers is given by the following ratios:

$$\frac{h_L}{h} = \frac{\Delta_L}{\Delta}\,\frac{\ell_L}{\ell}, \tag{43}$$

$$\frac{x_L}{x} = \frac{\ell_L}{\ell}, \tag{44}$$

$$\frac{t_L}{t} = \frac{\ell_L^2}{\ell^2}\,\frac{1-\lambda_L}{1-\lambda}\,\frac{D}{D_L}, \tag{45}$$

$$\frac{U_{pL}}{U_p} = \frac{\ell}{\ell_L}\,\frac{D_L}{D}\,\frac{\Delta_L}{\Delta}. \tag{46}$$

[56] Microscale and natural rivers have bed porosities with similar orders of magnitude: the porosity of microscale river beds is typically of the order of 0.35–0.4 whereas that of natural rivers varies in the range of 0.15–0.35 (R. Frings

Table 3. Comparison of Values for Several Natural Rivers to Those From an Experimental Run[a]

River	c_z	d (m)	Q (m^2s^{-1})	Re	x_L/x	h_L/h	t_L/t	U_{pL}/U_p	Δ_L/Δ
Elbow River	9.5	2.5×10^{-2}	1.3	1.3×10^{6}	9×10^{-6}	1.4×10^{-5}	2.6×10^{-6}	5.5	1.56
Oak Creek	4.5	1.8×10^{-2}	0.39	3.9×10^{5}	9×10^{-6}	1.5×10^{-5}	1.6×10^{-6}	9	1.62
North Saskatchewan River	11.4	3.2×10^{-2}	3.8	3.8×10^{6}	9×10^{-6}	2.4×10^{-5}	6.3×10^{-6}	3.8	2.63

[a]Chézy coefficient, median sediment diameter, average flow rate per unit width, average Reynolds number, x_L/x, h_L/h, t_L/t, U_{pL}/U_p, and Δ_L/Δ for several gravel bed rivers compared to one of our experimental runs performed with a flow rate of 1 L min^{-1} ($Q_L = 3.3 \times 10^{-4}$ m^2s^{-1}) and $Re = 333$. For the natural rivers, we consider a reach of characteristic length scale $\ell = 100$ km and we use the values of α and θ estimated by *Meyer-Peter and Müller* [1948]. Note that U_{pL}/U_p is merely computed to provide an example of rescaling. We do not imply that the Elbow River, Oak Creek, and North Saskatchewan River are subject to any active tectonics. Data are extracted from *Brownlie*'s [1981] and *Bagnold*'s [1980] databases.

et al., Discriminating between pore-filling load and bed-structure load: A new porosity-based method, exemplified for the river rhine, submitted to *Sedimentology*, 2008). Upscaling from a laminar to a turbulent river is therefore mainly controlled by the differences in the characteristic length scales, diffusion coefficients and threshold slopes. Figure 3 shows typical values of these last two parameters for both natural turbulent and microscale rivers. The threshold slope Δ_L of a laminar river varies between 10^{-3} and 10^{-2}, a range comparable to that of natural gravel bed rivers. Diffusion coefficients D_L for microscale rivers vary between 10^{-6} and 10^{-5} m^2s^{-1}. These values are 4–6 orders of magnitude smaller than those of natural rivers which are between 10^{-2} and 10 m^2s^{-1}. This means that natural rivers, for which length ℓ typically ranges between 10 and 1000 km, evolve on timescales varying between $(1 - \lambda)\ \ell^2/D \simeq 10^7$ and 10^{13}s, in other words between a few months and a few hundreds of thousands of years. The experimental laminar rivers, whose lengths are typically a few tens of centimeters, evolve on characteristic timescales $(1 - \lambda_L)\ \ell_L^2/D_L$ ranging between half an hour and a day. This difference is a reason for the keen interest in the use of microscale experiments.

[57] Developing equations (43)–(46) leads to

$$\frac{h_L}{h} = \left(\frac{\ell_L}{\ell}\right)\left(\frac{R_L d_L \theta_L}{R\, d\, \theta}\right)^{3/2}\left(\frac{Q/c_z}{\sqrt{3\nu_L Q_L}}\right), \tag{47}$$

$$\frac{x_L}{x} = \left(\frac{\ell_L}{\ell}\right), \tag{48}$$

$$\frac{t_L}{t} = \left(\frac{\ell_L}{\ell}\right)^2\left(\frac{1-\lambda_L}{1-\lambda}\right)\left(\frac{R_L/\alpha_L}{R/\alpha}\right)\left(\frac{Q/c_z}{\sqrt{3\nu_L Q_L}}\right), \tag{49}$$

$$\frac{U_{pL}}{U_p} = \left(\frac{\ell_L}{\ell}\right)^{-1}\left(\frac{R_L/\alpha_L}{R/\alpha}\right)^{-1}\left(\frac{R_L d_L \theta_L}{R\, d\, \theta}\right)^{3/2}. \tag{50}$$

These four equations can be used as calibration curves to compare a given experimental run with respect to a natural river. It is worth noting that h_L/h and t_L/t depend in particular on the flow rates per unit river width Q and Q_L whereas x_L/x and U_{pL}/U_p do not.

[58] Table 3 presents values of h_L/h, x_L/x, t_L/t and U_{pL}/U_p calculated for several natural rivers compared to one of our experimental run performed with a flow rate of 1 L per minute, that is $Q_L = 3.3.10^{-4}\ m^2s^{-1}$ and $Re = 333$. For the natural rivers, we consider a reach of characteristic length scale $\ell = 100km$ and we use the values of α and θ estimated by MeyerPeter and Müller. The laminar miscroscale river operates on a timescale typically 10^{-6} smaller than a natural one. Note that uplift rates are only 5 to 10 times faster in the lab than in nature. Such uplift rates would therefore be too small to be modeled using our experimental setup. Equation (50) shows that this situation can be solved by increasing the experimental grain size or reducing the microscale river length.

[59] From equations (43) and (44), it comes that the ratio of laminar to turbulent river bed slopes S_L/S goes as Δ_L/Δ. This ratio is larger than 1 (see Table 3) which explains why the slope of microscale rivers is larger than that of natural rivers.

[60] In the above discussion, we have implicitly assumed constant flow rates Q and Q_L. We now finish this section by examining how equations (47)–(50) can be used to upscale in the case of a variable flow rate. We will, as an example, consider the situation of a natural river subject to the influence of alternating floods and low flows so that the hydrograph can be written as

$$Q = Q_0\, f(t^*), \tag{51}$$

where Q_0 is some characteristic flow rate and $f(t^*)$ is a dimensionless function of the dimensionless time t^* describing the temporal variations of water flow rate. On the basis of equations (47) and (49), such an hydrograph is modeled in a microscale laminar river by applying a water flow rate with the following time dependency:

$$Q_L = Q_{L0}\, g\left(t_L^*\right)\ with\ g\left(t_L^*\right) = f(t^*)^2. \tag{52}$$

Q_{L0} is again some characteristic flow rate chosen by the experimenter and sets both h_L/h and t_L/t. The important result is that to model a field situation where Q goes as $f(t^*)$, one needs to apply Q_L going as $f(t_L^*)^2$ as illustrated on Figure 8. Note of course that this result holds true as long as the rate of change of water flow rate is not excessively high relative to the river adjustment timescale.

5. Conclusion

[61] In this paper, we have addressed the question of how to extrapolate results from the experimental microscale at which flow is laminar to the scale of natural turbulent rivers. In order to keep a simple analytical formalism, we restricted ourselves to the simplified case of a 2-D river of constant width.

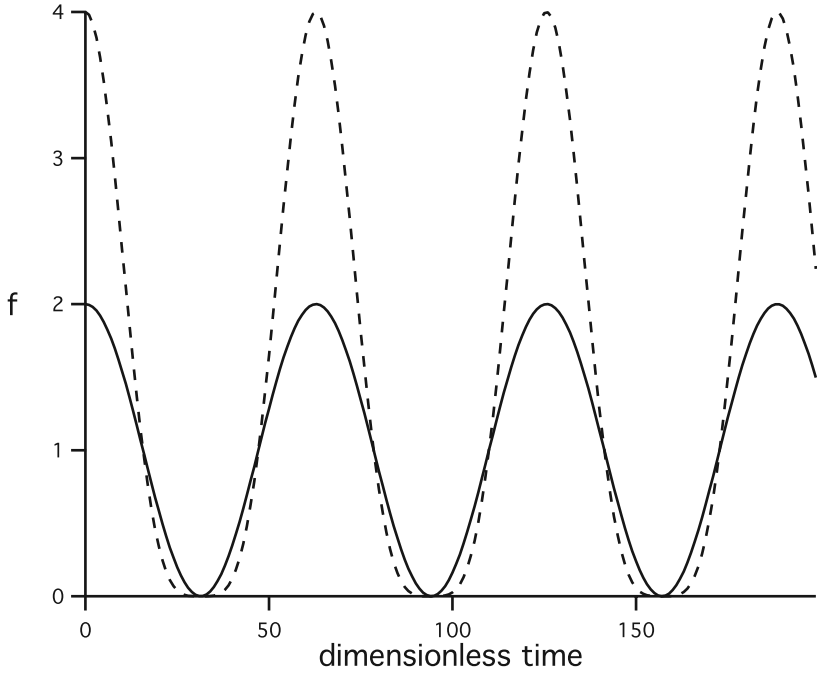

Figure 8. Hydrograph of $f(t^*)$ as a function of t^* (solid line) and $g(t_L^*)$ as a function of t_L^* (dashed line). We consider here the simple case of a sinusoidal hydrograph. But equation (52) holds regardless of the shape of the hydrograph.

[62] The use of microscale laminar rivers to model natural ones raises several questions: (1) the effect of surface tension which can become important at small length scale, (2) the modification of the friction equation, and (3) that of the sediment transport law with respect to the turbulent case. We have successively addressed all these points. First, we showed that surface tension is important only if the microscale river width is on the order of or smaller than the capillary length. Secondly, the friction equation was found to be correctly predicted from the Navier-Stokes equation solved for a steady uniform laminar flow. And finally we have shown experimentally that sediment transport in a microscale laminar river is consistent with *Meyer-Peter and Müller*'s [1948] transport model although the coefficients are different than in natural rivers. These results allowed us to demonstrate that the evolution of the longitudinal bed profile of a microscale laminar river is governed by a nonlinear diffusion equation successfully tested against experimental data.

[63] We then show that the evolution of longitudinal bed profiles of turbulent and laminar rivers are governed by identical dimensionless equations and therefore follow the same dynamics. Differences of time and length scales at work in experimental and natural rivers are mainly encoded in the expression of two parameters, a diffusion coefficient and a threshold slope. On the basis of this analysis, we derive a set of equations allowing to rescale bed elevation, downstream distance, time and uplift rate from an experimental microscale river to the field scale. Finally we show how this set of equations can be used to rescale these same parameters in the case of a time varying discharge, as long as the rate of change of the discharge is not excessively high.

[64] We do not imply that turbulence is irrelevant to the dynamics and morphology of alluvial rivers. Both the timescales of development and the spatial scales of expression can be expected to differ depending on whether the flow is laminar or turbulent. Several important classes of phenomena, such as suspended load and its related morphologies, are typically associated with turbulence and cannot be modeled in a laminar flow. To conclude, microscale experiments using laminar flow provide a valid, relatively quick and inexpensive method for investigating geological processes that occur on long timescales and for obtaining insights into many aspects of fluvial morphodynamics.

[65] **Acknowledgments.** We thank Y. Gamblin and A. Vieira for their technical assistance in designing and realizing the experimental setup. We are indebt to C. Jaupart and O. Devauchelle for many fruitful discussions and to M. Tal for her corrections to the manuscript. This is IPGP contribution 2367.

References

Allen, J. (1985), *Principles of Physical Sedimentology*, Blackburn Press, Caldwell, N. J.

Ashworth, P., J. Best, J. Leddy, and G. Geehan (1994),The physical modelling of braided rivers and deposition of fine-grained sediment, in *Process Models and Theoretical Geomorphology*, edited by M. J. Kirkby, pp. 115–139, John Wiley, Chichester, U. K.

Bagnold, R. (1980), An empirical correlation of bedload transport rate in flumes and natural rivers, *Proc. R. Soc. Lond. Ser. A*, *372*, 453–473.

Begin, Z., D. Meyer, and S. Schumm (1981), Development of longitudinal profiles of alluvial channels in response to base level lowering, *Earth Surf. Processes Landforms*, *6*, 49–68.

Blom, A., J. S. Ribberink, and H. J. de Vriend (2003), Vertical sorting in bed forms: Flume experiments with a natural and a trimodal sediment mixture, *Water Resour. Res.*, *39*(2), 1025, doi:10.1029/2001WR001088.

Brownlie, W. (1981), Compilation of alluvial channel data: Laboratory and field, tech. rep., W. M. Keck Lab. of Hydraul. and Water Resour., Calif. Inst. of Technol., Pasadena, Calif.

Bryant, M., P. Falk, and C. Paola (1995), Experimental study of avulsion frequency and rate of deposition, *Geology*, *23*, 365–368.

Cantelli, A., C. Paola, and G. Parker (2004), Experiments on upstream-migrating erosional narrowing and widening of an incisional channel caused by dam removal, *Water Resour. Res.*, *40*, W03304, doi:10.1029/2003WR002940.

Carling, P. A., K. Richardson, and H. Ikeda (2005), A flume experiment on the development of subaqueous fine-gravel dunes from a lower-stage plane bed, *J. Geophys. Res.*, *110*, F04S05, doi:10.1029/2004JF000205.
Carson, M., and G. Griffiths (1987), Bedload transport in gravel channels, *J. Hydrol. New Zealand*, *26*, 1–151.
Charru, F., H. Mouilleron, and O. Eiff (2004), Erosion and deposition of particles on a bed sheared by a viscous flow, *J. Fluid Mech.*, *519*, 55–80.
Davies, T., M. McSaveney, and P. Clarkson (2003), Anthropic aggradation of the Waiho River, Westland, New Zealand: Microscale modeling, *Earth Surf. Processes Landforms*, *28*, 209–218.
Degennes, P. (1985), Wetting: Statics and dynamics, *Rev. Mod. Phys.*, *57*(3), 827–863.
Dietrich, W., D. Bellugi, L. Sklar, J. Stock, A. Heimsath, and J. Roering (2003), Geomorphic transport laws for predicting landscape form and dynamics, in *Prediction in Geomorphology*, *Geophys. Monogr. Ser.*, vol. 135, edited by P. Wilcox and R. Iverson, pp. 103–132, AGU, Washington D. C.
French, R. (1985), *Open-Channel Hydraulics*, McGraw-Hill, New York.
Gessler, J. (1971), Aggradation and degradation, in *River Mechanics*, vol. 1, edited by H. Shen, pp. 8-1–8-24, Fort Collins, Colorado.
Gomez, B., and M. Church (1989), An assessment of bed load sediment transport formulae for gravel bed rivers, *Water Resour. Res.*, *25*, 1161–1186.
Graf, W., and M. Altinakar (1996), *Hydraulique Fluviale: Ecoulement non Permanent et Phenomenes de Transport*, Eyrolles, Paris.
Guyon, E., J. Hulin, and L. Petit (2001), *Hydrodynamique Physique*, EDP Sci., Les Ulis, France.
Hong, L., and T. Davies (1979), A study of stream braiding, *Geol. Soc. Am. Bull.*, *90*, 1094–1095.
Hooke, R. (1968), Model geology; Prototype and laboratory streams; Discussion, *Geol. Soc. Am. Bull.*, *79*, 391–394.
Jones, S., and L. Frostick (2008), Inferring bedload transport from stratigraphic successions: Examples from Cenozoic and Pleistocene rivers, south central Pyrenees, Spain, *Geol. Soc. Spec. Publ.*, *296*, 129–145.
Keulegan, G. (1938), Laws of turbulent flow in open channels, *Res. Pap. RP 1151*, Natl. Bur. of Stand., Boulder, Colo.
Kim, W., and T. Muto (2007), Autogenic response of alluvial-bedrock transition to base-level variation: Experiment and theory, *J. Geophys. Res.*, *112*, F03S14, doi:10.1029/2006JF000561.
Knighton, D. (1998), *Fluvial Forms and Processes: A New Perspective*, Hodder Arnold, London.
Koss, J., F. Ethridge, and S. Schumm (1994), An experimental study of the effects of base-level change on fluvial, coastal plain, and shelf systems, *J. Sediment. Res.*, *B64*, 90–98.
Kostaschuk, R., M. Church, and J. Luternauer (1989), Bedforms, bed material, and bedload transport in a salt-wedge estuary: Fraser River, British Columbia, *Can. J. Earth Sci.*, *26*(7), 1440–1452.
Lajeunesse, E., and B. Homsy (2003), Thermocapillary migration of long bubbles in polygonal tubes. Part II: Experiments, *Phys. Fluids*, *15*, 308–314, doi:10.1063/1.1531617.
Lisle, T., J. Pizzuto, H. Ikeda, F. Iseya, and Y. Kodama (1997), Evolution of a sediment wave in an experimental channel, *Water Resour. Res.*, *33*, 1971–1981.
Liu, Y., F. Metivier, E. Lajeunesse, P. Lancien, C. Narteau, and P. Meunier (2008), Measuring bed load in gravel bed mountain rivers: Averaging methods and sampling strategies, *Geodin. Acta*, *21*, 81–92.
Malverti, L., E. Lajeunesse, and F. Metivier (2007), Experimental investigation of the response of an alluvial river to a vertical offset of its bed, in *River, Coastal and Estuarine: 5th IAHR Symposium Morphodynamics*, edited by S. Huslcher and C. Dohmen-Janssen, pp. 179–184, Taylor and Francis, Philadelphia, Pa.
Métivier, F. (1999), Diffusivelike buffering and saturation of large rivers, *Phys. Rev. E.*, *60*(5), 5827–5832.
Métivier, F. (2003), Des sources aux océans: Enjeux et problématiques en géomorphologie fluviale, thèse d'habilitation á diriger des recherches, Université Paris Diderot, Paris.
Métivier, F., and P. Meunier (2003), Input and output mass flux correlations in an experimental braided stream: Implications on the dynamics of bed load transport, *J. Hydrol.*, *271*(1–4), 22–38.
Métivier, F., P. Meunier, M. Moreira, A. Crave, C. Chaduteau, B. Ye, and G. Liu (2004), Transport dynamics and morphology of a high mountain stream during the peak flow season: The ürümqi River (Chinese Tianshan), in *River Flow 2004: Proceedings of the Second International Conference on Fluvial Hydraulics*, edited by M. Greco et al., pp. 761–777, Taylor and Francis, Philadelphia, Pa.
Meunier, P., and F. Metivier (2000), Permanent transport regime of an experimental braided river, *C. R. Acad. Sci. Ser. IIaSci. Terre Planetes*, *331*(2), 105–110.
Meunier, P., and F. Metivier (2006), Sediment transport in a microscale braided stream: From grain size to reach size, in *Braided River, Process, Deposits, Ecology, and Management*, edited by G. Sambrook-Smith et al., pp. 212–226, Blackwell, Malden, Mass.
Meunier, P., F. Metivier, E. Lajeunesse, A. S. Meriaux, and J. Faure (2006), Flow pattern and sediment transport in a braided river: The "torrent de St Pierre" (French Alps), *J. Hydrol.*, *330*(3–4), 496–505.
Meyer-Peter, E., and R. Müller (1948), Formulas for bed-load transport, in *Proceedings 2nd Congress International Association of Hydraulic Research*, pp. 39–64, Int. Assoc. of Hydraul. Res., Stockholm.
Muto, T., and J. B. Swenson (2005), Large-scale fluvial grade as a nonequilibrium state in linked depositional systems: Theory and experiment, *J. Geophys. Res.*, *110*, F03002, doi:10.1029/2005JF000284.
Nezu, I., and H. Nakagawa (1993), *Turbulence in Open-Channel Flows*, Balkema, Rotterdam, Netherlands.
Owen, M. (1985), Ports and harbour, in *Developments in Hydraulic Engineering—3*, edited by P. Novak, pp. 263–311, Elsevier, London.
Paola, C. (2000), Quantitative models of sedimentary basin filling, *Sedimentology*, *47*, 121–178.
Paola, C., P. Hellert, and C. Angevine (1992), The large-scale dynamics of grain-size variation in alluvial basins, part 1: Theory, *Basin Res.*, *4*, 73–90.
Paola, C., et al. (2001), Experimental stratigraphy, *GSA Today*, *11*(7), 4–9.
Parker, G. (1978a), Self-formed straight rivers with equilibrium banks and mobile bed. Part 1: The sand-silt river, *J. Fluid Mech.*, *89*, 109–125.
Parker, G. (1978b), Self-formed straight rivers with equilibrium banks and mobile bed. Part 2: The gravel river, *J. Fluid Mech.*, *89*, 127–146.
Parker, G. (1991), Selective sorting and abrasion of river gravel. Part II: Applications, *J. Hydraul. Eng.*, *117*, 150–171.
Parker, G. (1999), Progress in the modelling of alluvial fans, *J. Hydraul. Res.*, *37*, 805–825.
Parker, G., C. Paola, K. Whipple, D. Mohrig, C. Toro-Escobar, M. Halverson, and T. Skoglund (1998), Alluvial fans formed by channelized fluvial and sheet flow. Part II: Application, *J. Hydraul. Eng.*, *124*, 996–1004.
Peakall, J., and J. Warburton (1996), Surface tension in small hydraulc river models—The significance of the weber number, *J. Hydrol. New Zealand*, *35*, 199–212.
Peakall, J., P. Ashworth, and J. Best (1996), Physical modelling in fluvial geomorphology: Principles, applications, and unresolved issues, in *The Scientific Nature of Geomorphology*, edited by B. Rhoads and C. Thorn, pp. 221–253, John Wiley, Chichester, U. K.
Peakall, J., P. Ashworth, and J. Best (2007), Meander-bend evolution, alluvial architecture, and the role of cohesion in sinuous river channels: A flume study, *J. Sediment. Res.*, *77*, 197–212, doi:10.2110/jsr.2007.017.
Raudkivi, A. (1990), *Loose Boundary Hydraulics*, Pergamon, New York.
Sapozhnikov, V., and E. Foufoula-Georgiou (1997), Experimental evidence of dynamic scaling and indications of self-organized criticality in braided rivers, *Water Resour. Res.*, *33*, 1983–1991.
Schumm, S., M. Mosley, and W. Weaver (1987), *Experimental Fluvial Geomorphology*, John Wiley, New York.
Shields, I. (1936), Anwendung der ahnlichkeitmechanik und der turbulenzforschung auf die gescheibebewegung, *Rep. 26*, Mitt. Preuss Ver. Anst., Berlin.
Sklar, L., W. Dietrich, E. Foufoula-Georgiou, B. Lashermes, and D. Bellugi (2006), Do gravel bed river size distributions record channel network structure?, *Water Resour. Res.*, *42*, W06D18, doi:10.1029/2006WR005035.
Straight, B. (1992), The water flow and building behaviour of a small alluvial fan, M.Sc. thesis, Lincoln University, Christchurhc, New Zealand.
Whipple, K., G. Parker, C. Paola, and D. Mohrig (1998), Channel dynamics, sediment transport and the slope of alluvial fans: Experimental study, *J. Geol.*, *106*, 677–693.
Wohl, E. (2000), *Mountain Rivers*, *Water Resour. Monogr. Ser.*, vol. 14, AGU, Washington, D. C.
Wong, M. (2003), Does the bedload equation of Meyer-Peter and Müller fit its own data?, paper presented at 30th Congress, Int. Assoc. of Hydraul. Res., Thessaloniki, Greece.
Wright, S., and G. Parker (2004), Flow resistance and suspended load in sand-bed rivers: simplified stratification model, *J. Hydraul. Eng.*, *130*, 796–805.
Yalin, M. (1977), *Mechanics of Sediment Transport*, Pergamon, New York.
Yalin, M. (1992), *River Mechanics*, Pergamon, New York.

E. Lajeunesse, L. Malverti, and F. Métivier, Laboratoire de Dynamique des Fluides Géologiques, Institut de Physique du Globe de Paris, 4 place Jussieu, F-75252 Paris CEDEX 05, France. (lajeunes@ipgp.jussieu.fr)